Strong ground motion from the seismic swarms preceding the 2021 and 2022 volcanic eruptions at Fagradalsfjall, Iceland

Victor M. Hernández-Aguirre[1,2] · Rajesh Rupakhety[1,2] · Simon Ólafsson[1,2] · Bjarni Bessason[1] · Sigurður Erlingsson[1] · Roberto Paolucci[3] · Chiara Smerzini[3]

Abstract: The Geldingadalir and Meradalir eruptions at Mt. Fagradalsfjall in the Reykjanes Peninsula on 19 March 2021 and 3 August 2022, respectively, were preceded by intense volcano-tectonic swarms. Eight earthquakes with M≥5 were recorded by the Icelandic Strong Motion Network. We present an overview of the seismicity in Fagradalsfjall, and salient features of the strong ground motion caused by the swarms in the epicentral area. The largest recorded horizontal Peak Ground Acceleration (PGA) was ~0.45g at Grindavík, which is the strongest PGA recorded in Iceland since the M_W6.3 2008 Ölfus Earthquake. Recorded waveforms show a rich long-period energy content, with a burst of higher frequencies at the beginning of shaking. This leads to larger response spectral accelerations at long periods that those from typical shallow crustal earthquakes. Moreover, an empirical mixed-effects ground motion model for PGA, PGV and PSA was calibrated for rock sites based on the available recordings. The attenuation rate from this model is similar to that introduced by Lanzano and Luzi (2020) which is based on data from volcanic events in Italy, but the magnitude scaling of our model is much lower. The overall results indicate that scaling and attenuation of ground motion from volcanic events and purely tectonic earthquakes in Iceland are different. This is an important observation because seismic hazard in parts of the Reykjavik area and of the central highlands, where important hydroelectric power plants are located, could potentially be dominated by events of volcanic origin. Therefore, it is important to take these observations into account for seismic hazard and risk assessment in Iceland.

Keywords: IceSMN; Fagradalsfjall; Iceland eruption; Volcano-tectonic earthquake; Earthquake swarm; Ground Motion Model (GMM).

1 Introduction

Unrest in the Reykjanes Peninsula was first identified in Mt. Þorbjörn-Svartsengi in mid-January 2020, when inflation of about 3-4 mm/day was detected in automated Global Navigation Satellite System (GNSS) and Synthetic Aperture Radar Interferometry (InSAR) observations, coinciding with the onset of an earthquake swarm (Geirsson et al., 2021). In the volcanic system Krýsuvík, 20 km east of Svartsengi, inflation started in August 2020, leading to a M5.6 earthquake on 20 October 2020.

In February 2021, crustal extension and an intense earthquake swarm revealed the formation of an ~8-km-long NE-SW striking magmatic dyke between Svartsengi and Krýsuvík (Flóvenz et al., 2022), that propagated to the surface to feed the Geldingadalir eruption at Mt. Fagradalsfjall on 19 March 2021 (see Fig. 1). The eruption lasted 6 months and produced a lava field covering an area of 4.8 km^2 with an extruded bulk volume of $150\pm3\times10^6$ m^3(Pedersen et al., 2022).

The 2021 Geldingadalir eruption was the first to occur on the Reykjanes Peninsula since the 13th century episode that affected both the Reykjanes and Svartsengi volcanic systems (Sæmundsson et al., 2020). This eruption was the first in the Fagradalsfjall system in at least 6000 years (Sæmundsson et al., 2016). In the Reykjanes Peninsula, periods of rifting and volcanism occur at intervals of 800–1000 years (Sæmundsson et al., 2020) alternating with periods of predominant transcurrent motion manifested as high seismicity episodes occurring at intervals of a few tens of years (Einarsson, 2008).

The intense swarm preceding the eruption started on 24 February. A total of ~4000 earthquakes with local moment magnitude (see details in Section 3) $M_{LW}>1$ were reported by the Icelandic Meteorological Office, IMO, from 24 February to 19 March 2021 in the Fagradalsfjall area (IMO, 2022a). Six events had a magnitude

✉ R. Rupakhety
   rajesh@hi.is

[1] Earthquake Engineering Research Center, University of Iceland, Selfoss, Iceland

[2] Faculty of Civil and Environmental Engineering, University of Iceland, Reykjavík, Iceland

[3] Department of Civil and Environmental Engineering, Politecnico di Milano, Milan, Italy

M≥5, as shown in Fig.1. The Icelandic Strong Motion Network (IceSMN) operated by the Earthquake Engineering Research Centre (EERC) of the University of Iceland recorded ground accelerations caused by these events. Stations as close as ~4km and as far as ~300km were triggered by these events. The M5.7 earthquake on 24 February is the largest recorded in the Peninsula since 2000 (Jónasson et al., 2021).

The unrest in the Peninsula continued after the end of the Geldingadalir eruption. In December 2021, a short swarm was detected again in Fagradalsfjall, with the largest event having a magnitude of 4.8. Inflation in Mt. Þorbjörn-Svartsengi was detected again in April and May 2022. Then, another strong swarm started in Fagradalsfjall on 30 July 2022. The largest event from this swarm was a M5.4 earthquake on 31 July 2022, that caused a horizontal peak ground acceleration (PGA) of ~0.45 g at station Grindavík (GRI). This is the strongest recorded shaking in Iceland since the 2008 Ölfus Earthquake. Magmatic intrusion was reported in Fagradalsfjall on 1 August 2022 (IMO, 2022b), and eventually a new eruption started on 3 August 2022, known as Meradalir eruption, just approximately 1 km northeast of the Geldingadalir eruption site (Fig. 1). Fresh lava was last emitted on 21 August 2022.

This work presents an overview of the seismicity on the Reykjanes Peninsula from January 2020 to August 2022. Furthermore, salient features of strong ground motion recorded during the intense earthquakes preceding the 2021 Geldingadalir and 2022 Meradalir eruptions are presented. This is the first time that broad-band near-fault accelerograms from M>5 volcano-tectonic earthquakes are recorded in Iceland. Such accelerograms are rare also in the international context. This data allows, for the first time, a quantitative comparison of the scaling and attenuation of ground motion from volcano-tectonic and purely tectonic earthquakes in Iceland. Comparison of the scaling and attenuation of ground motion from these events in Iceland to those recorded elsewhere provides additional value and insight on the nature of ground motion modelling in volcano-tectonic environments. It is important to report these observations and their deviation from data based on tectonic seismicity. The discrepancy must be accounted for in seismic hazard and risk assessment in Iceland.

2 Tectonic framework

The Reykjanes Peninsula rift (Fig. 1) is a segment of the mid-Atlantic plate boundary and forms a transition between the Reykjanes Ridge off shore to the west and the Western Volcanic Zone and the South Iceland Seismic Zone to the east (Einarsson, 1991). The plate boundary as shown by the epicentral zone of earthquakes runs along the peninsula in the direction of about N(70-80)°E (Björnsson et al., 2020; Keiding et al., 2009), whereas the relative spreading of the North American and Eurasian Plates is about ~18–19 mm/year in direction ~N(100–105)°E, as measured from a global plate motion model, MORVEL2010 (DeMets et al., 2010), and GNSS geodesy (Sigmundsson et al., 2020). The oblique spreading leads to extensive volcanism and large earthquakes (Einarsson, 2008).
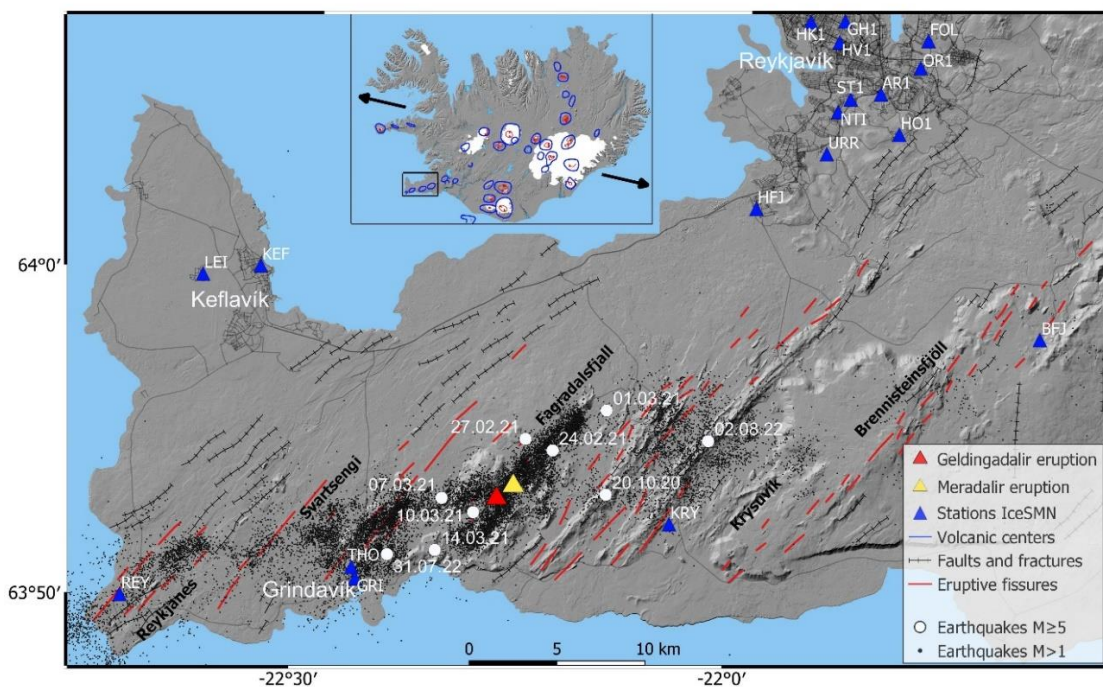
Fig. 1. Map of the Reykjanes Peninsula. The red and yellow triangles indicate the location of the Geldingadalir 2021 and Meradalir 2022 eruptions, respectively. The dots show the seismicity from 01.01.2021 to 31.08.2022 as reported by IMO. Blue triangles are the accelerometric stations of the IceSMN network. Faults, fractures, eruptive fissures, and volcanic systems are also presented (Jóhannesson & Sæmundsson, 2009). The Iceland inset on top shows the location of the Reykjanes Peninsula (black square), as well as the direction of the spreading between the North American and Eurasian tectonic plates represented by the black arrows.

The main tectonic features on the peninsula are a large number of NE-SW trending volcanic fissures and normal faults and a series of N-S oriented right-lateral strike-slip faults (Clifton & Kattenhorn, 2006). As shown in Fig. 1, there are six volcanic systems in the peninsula (Sæmundsson et al., 2020), namely: Reykjanes, Svartsengi, Fagradalsfjall, Krýsuvík, Brennisteinsfjöll and Hengill. The fissure swarms of the volcanic systems extend a few tens of kilometres into the plates on either side, have a trend of about N35°E, and are thus arranged en echelon with respect to the plate boundary (Einarsson, 2008).

Seismic activity on the peninsula is episodic. Recent high activity periods took place at the beginning of the last century, in 1929–1935, 1967–1975, 2000–2004 (Björnsson et al., 2020; Einarsson, 2008), and 2017(Hrubcová et al., 2021). The largest earthquakes in the latest episodes were associated with strike-slip faulting (Árnadóttir et al., 2004; Einarsson, 1991). Hreinsdóttir et al. (2001) suggest that transcurrent motion is taken up by right-lateral motion on N-S trending strike-slip faults (Einarsson et al., 1981) while extension perpendicular to the fissure swarms takes place during magmatic periods by dyke injection. In the period 1900-2019, 25 earthquakes of $M_W \geq 5$ occurred on the Peninsula, west of −22°0' (Fig. 1), i.e., on average one earthquake every fifth year, according to the ICEL-NMAR earthquake catalogue (Jónasson et al., 2021). The catalogue can be assumed to be complete for this size of earthquakes from 1915.

3 Seismicity in Fagradalsfjall between 2020 and 2022

3.1 Earthquake magnitude

The IMO earthquake catalogue is based on the SIL (South Iceland Lowland) seismic network, which has been operating since 1991 (Böðvarsson et al., 1996, 1999; Stefánsson et al., 1993). The network was initially installed in South Iceland but gradually expanded to cover all geologically active areas in the country. By 2020, around 80 stations were operating in the SIL-network (Jónasson et al., 2021). Earthquake locations and local magnitudes are automatically computed and then manually reviewed and adjusted when necessary. Focal mechanisms and seismic moments (M_0) are obtained by grid searching over all combinations of strike, dip and rake, matching observed first-motion polarities as well as amplitudes of P, SV and SH waves estimated from spectral analysis of short data segments containing the direct waves arrivals (Rögnvaldsson & Slunga, 1993).

The IMO catalogue reports two magnitude estimates. The first one, M_L, is based on an empirical local magnitude relationship, while the second is a local moment magnitude, M_{LW} (Rögnvaldsson & Slunga, 1993), computed from the M_0 estimate with a set of equations that can be found in the appendix I of Pétursson & Vogfjörð (2009). Fig. 2 compares the local magnitudes reported by IMO and their corresponding magnitude estimates reported by GCMT (Dziewonski et al., 1981; Ekström et al., 2012) for all the events with Mw>4.5 in the Reykjanes Peninsula between 01 January 2020 and 31 August 2022. M_L is always lower than Mw. The M_{LW} estimate is similar to M_w for events with M_w>4.7. For smaller events, M_{LW} tends to be smaller than Mw. Since the focus in this work is on larger events causing strong motion, we use the M_{LW} as a reference for earthquake size, that, for simplicity, will be denoted in the following by M.

Fig. 2 Comparison between the local magnitudes reported by the IMO (local M_L, represented by blue dots, and local moment magnitude M_{LW}, represented by red dots), and moment magnitude, Mw, reported by GCMT for all the events with Mw>4.5 that took place in the Reykjanes Peninsula between 01 January 2020 and 31 August 2022.
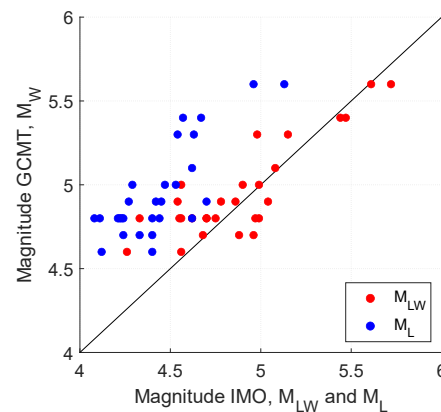
The differences between M_L and M_{LW}, evident in Fig. 2 and more notorious as magnitude increases, have been previously explained by the fact that the SIL system's analysis is optimised towards robust magnitude estimation of smaller earthquakes. Furthermore, M_L underestimates large magnitudes because high-pass filtered (f>1.5 Hz) velocity amplitudes from short-period seismometers are used for its computation (e.g., Jónasson et al., 2021; Panzera et al., 2016).

3.2 Frequency and spatial distribution

The seismicity in the Reykjanes Peninsula between 01 January 2020 and 31 August 2022 was characterized by various swarms of volcano-tectonic origin lasting from a few days to almost one month. Most of the earthquakes in this period were located in the Fagradalsfjall volcanic system, forming two clusters close the eruption sites. The NE-SW trending cluster maps the dyke propagation, while the WSW-ENE trending cluster follows the plate boundary (see Fig. 1). According to Fischer et al. (2022), the magma erupted at a place of crustal weakening under tension at the intersection of the WSW-ENE trending cluster with the dyke.

In this section we focus on the seismicity in the Fagradalsfjall area, that runs from parallels 63°51'N to 63°57'N, and meridians 22°W to 22°24'W, as shown in Fig. 3. This is a wilderness area with no population. The closest built environment is Grindavík, which is a fishing village with a population of 3500. The cumulative number of earthquakes with M>1 in Fagradalsfjall from January 2020 to September 2022 are shown in Fig. 4a. On 24 February 2021, there was a sharp increase in seismicity, reflected by the intense swarm that took place prior to the Geldingadalir eruption. From 24 February 2021 to 19 March 2021, ~4000 earthquakes with M>1 were reported by IMO in the Fagradalsfjall area. In October 2021, after the last emission of fresh lava on 18 September 2021, there was again an increase of seismicity clustered in the NE corner. On 22 December 2021 a new swarm was detected, also evident in Fig. 4a, forming a NE-SW trending cluster coinciding with the dyke previously formed. The largest earthquakes in this swarm were the M4.8 on 22 December and the M4.7 on Christmas Eve. Finally, another sharp increase in seismicity is observed on 30 July 2022, related to the strong swarm preceding the Meradalir eruption. During this swarm, 358 earthquakes with M>1 were reported by IMO, 2 of which had M>5.
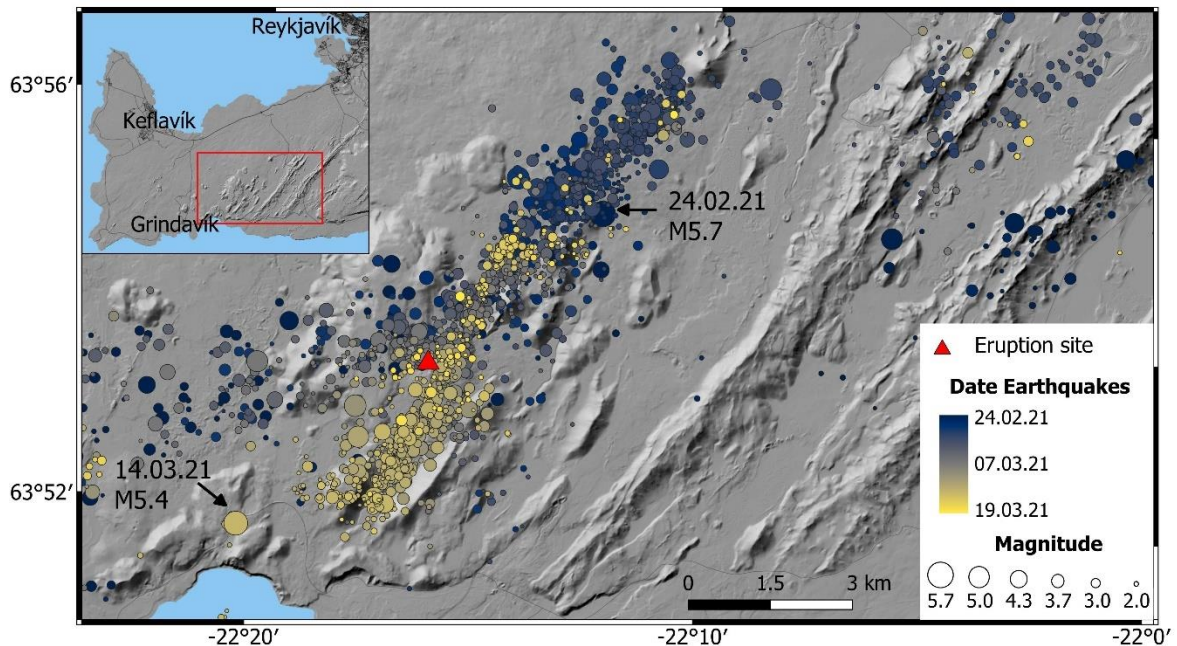

Fig. 3 The February-March 2021 swarm in Fagradalsfjall. Earthquakes with M>2 are presented and they are colour coded according to the date of occurrence.

The frequency-magnitude distribution (FMD) of earthquakes during this period is presented in Fig. 4b. The Gutenberg–Richter model (Gutenberg & Richter, 1944) that fits the cumulative FMD, shown with the red line, is also shown. The magnitude of completeness is taken as the minimum magnitude for which the goodness-of-fit (Wiemer & Wyss, 2000) was larger than 93%. The maximum likelihood formulation (Aki, 1965) is used to estimate the b- and a-values of the Gutenberg-Richter model. The results show that the slope parameter (b-value) is equal to 1.0, which is slightly higher than an estimate of 0.91 from a previous study for the same area (Kieding et al., 2009). The seismicity parameter, represented by the a-value is rather large. There were 92

events with M>4 for this period of 2 years and 8 months, or 34.5 events per year, while for the same area there were just 13 events of M>4 from 2000 to 2020, i.e., 0.62 events per year (Jónasson et al., 2021).
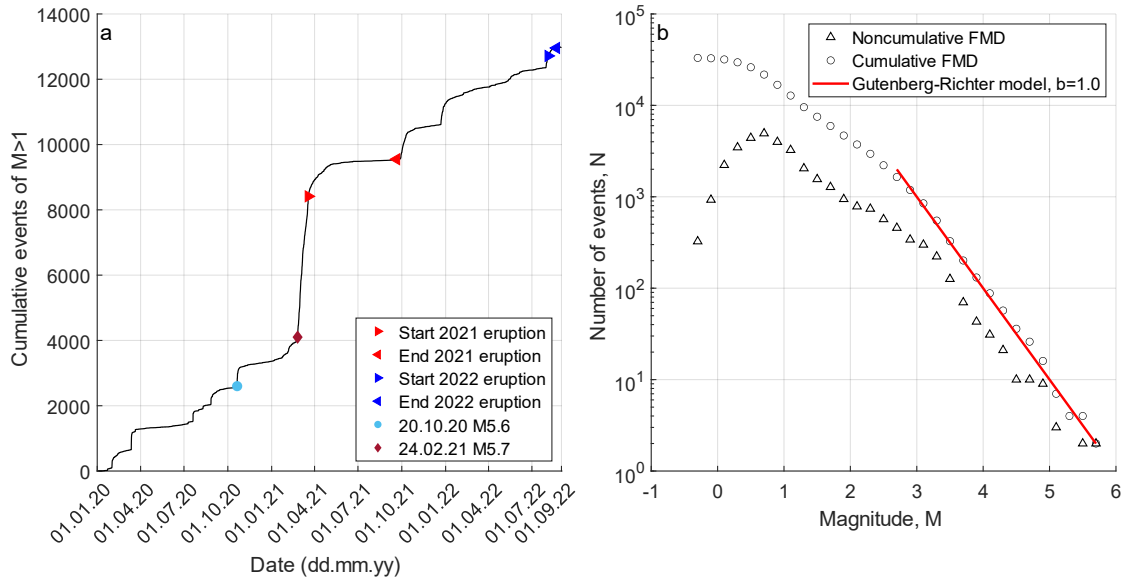

Fig. 4 a) Time series of cumulative number of earthquakes with magnitude M>1 for the Fagradalsfjall area. b) Frequency-magnitude distributions for the same period. Red line represents the fitting of the data with the Gutenberg–Richter model.

The seismicity in Fig. 3 shows the propagation of the dyke, which started at its north-east end. The largest event of the swarm, a M5.7 earthquake (M_W5.6 according to USGS and GCMT), occurred at 10:05h UTC on 24 February 2021, and it was preceded by 3 hours of intense microearthquake activity occurring in a narrow 7 km depth zone, suggesting the start of the magmatic intrusion (Sigmundsson et al., 2022). On 27 February and 1 March earthquakes of M5.1 and M5.0, respectively, occurred NE of the eruption site. Then, the seismicity migrated south-westward. Three earthquakes with M≥5 occurred south-west of the eruption site, on 7, 10 and 14 March. Finally, the seismicity jumped back to the central part where the effusive eruption eventually occurred on 19 March 2021. Sigmundsson et al. (2022) report a deformation and seismicity decline few days before the eruption onset, possibly related to the weaker crust near the surface, as the depth of active magma emplacement progressively shallowed.

3.3 Focal mechanisms

The focal mechanisms reported by USGS (2022) and GCMT (Dziewonski et al., 1981; Ekström et al., 2012) for seven of the earthquakes with M≥5 are presented in Table 1. In general, the large events had an almost N-S right-lateral strike-slip faulting with a small normal component. This type of faulting is common for large events in the Reykjanes Peninsula (Árnadóttir et al., 2004; Björnsson et al., 2020; Einarsson, 1991).

Table 1 Focal mechanisms reported by USGS and GCMT for 6 earthquakes from the 2021 February-March swarm and the largest event of the 2022 July-August swarm. The depth (H) is taken from IMO (2022a).

		24.02.21	27.02.21	01.03.21	07.03.21	10.03.21	14.03.21	31.07.22
USGS	M_W	5.6	5.2	4.9	5.3	5.1	5.3	5.4
	Strike (°)	182	4	-	356	16	0	359
	Dip (°)	78	65	-	79	67	42	38
	Rake (°)	-155	-157	-	-141	-137	-152	-161
GCMT	M_W	5.6	5.3	5.0	5.3	5.1	5.4	5.4
	Strike (°)	358	360	6	353	3	357	357
	Dip (°)	89	89	85	82	87	87	87
	Rake (°)	-170	-171	-159	-161	-165	-165	-161
	H (km)	1.2	4.8	2.6	6.6	5.8	3.1	2.7

The N-S striking fault planes can be explained by the Riedel shear model (Fischer et al., 2022), for which the shear on the left-lateral transform fault at the approximately N75°E plate boundary is decomposed into

5

synthetic R and antithetic R' shear fractures. Antithetic R' are approximately N-S, coinciding with the N-S fault planes. According to this model tensile fractures should develop at ∼N40°E, that matches the NE-SW dyke emplacement.

4 Strong ground motion

During the 2021 February-March and the 2022 July-August swarms in the Reykjanes Peninsula, eight earthquakes with a magnitude 5 or larger were reported by IMO. Their epicentres are marked in Fig. 1 with white circles. Ground accelerations for these events were recorded by the IceSMN. In this section we report the ground motion caused by some of these earthquakes.

4.1 Ground motion recordings

The three components of PGA recorded at 6 stations of the IceSMN in the Reykjanes Peninsula (see locations in Fig. 1) are presented in Table 2. Bold values are the PGA's that exceeded the 475-year return period PGA of 0.2 g, used for seismic design in Grindavík and the surrounding areas (SI, 2010). It can be observed that during the three largest earthquakes, the design PGA was exceeded at the three closest stations, i.e., Krýsuvík (KRY), Grindavík (GRI) and Þorbjörn (THO). The largest PGA was recorded during the 31 July M5.4 earthquake at GRI, where it reached 0.45g, which is more than twice the design PGA. Rock falls, pipeline breakage (RUV, 2022a), and non-structural damages (RUV, 2022b) were reported after this earthquake.

Table 2 PGA values for the north-south (N-S), east-west (E-W) and up-down (U-D) components recorded at 6 stations of the IceSMN during the largest events of the 2021 February-March and 2022 July-August swarms. The epicentral distance (R_{epi}) is also shown. Bold values are those exceeding the 475-year return period PGA.

Station	Comp	24.02.21 M5.7		27.02.21 M5.1		10.03.21 M5.1		14.03.21 M5.4		31.07.22 M5.4	
		R_{epi} [km]	PGA [g]	R_{epi} [km]	PGA [g]	R_{epi} [km]	PGA [g]	R_{epi} [km]	PGA [g]	R_{epi} [km]	PGA [g]
KRY	N-S		**0.244**		0.095		0.048		0.040		0.019
	E-W	7.8	**0.395**	9.5	0.133	13.3	0.030	13.3	0.045	16.0	0.028
	U-D		**0.288**		0.045		0.013		0.019		0.012
GRI	N-S		0.048		0.027		0.023		**0.203**		**0.456**
	E-W	13.3	0.060	12.4	0.038	4.7	0.016	4.7	0.143	1.9	**0.274**
	U-D		0.040		0.021		0.053		0.077		**0.203**
BFJ	N-S		0.008		0.004		0.003		0.004		0.004
	E-W	28.3	0.012	29.7	0.004	36.3	0.004	36.3	0.005	39.1	0.004
	U-D		0.008		0.004		0.003		0.004		0.004
THO	N-S		0.085		0.068		0.140		**0.263**		**0.451**
	E-W	13.2	0.105	12.3	0.078	4.8	0.061	4.8	**0.296**	2.2	**0.336**
	U-D		0.047		0.036		0.045		0.137		**0.277**
HFJ	N-S		0.038		0.170		0.014		0.015		0.015
	E-W	17.9	0.029	18.5	0.016	26.6	0.008	26.6	0.011	29.2	0.019
	U-D		0.044		0.011		0.005		0.009		0.008
KEF	N-S		0.026		0.009		0.010		0.017		0.021
	E-W	19.6	0.016	17.9	0.010	18.9	0.013	18.9	0.023	18.8	0.028
	U-D		0.017		0.007		0.011		0.017		0.019

Fig. 5 and Fig. 6 show the acceleration and velocity time series, respectively, recorded during the three largest events for the same six stations mentioned before. It is worth nothing that stations GRI and THO are just ~650 m apart (see Fig. 1), but experienced very different ground acceleration. Ground velocities at these two stations are similar in peak amplitude except the high frequency oscillations at THO. The differences between these two stations are more contrasting when comparing their elastic response spectra, as it will be shown in the next section. Even though, according to the Geological map of SW Iceland (Sæmundsson et al., 2016), both stations are located on postglacial lavas, we believe that local site effects at THO are the main reason for such difference.

While, for almost all stations and earthquakes, the vertical and horizontal PGAs are similar, the vertical component of velocity is in general lower (see Fig. 6), indicating, as clearly visible in Fig. 5, that the vertical component is richer in higher frequencies than the horizontal ones, as expected from empirical studies available in the literature (e.g., Ramadan et al., 2021). Also, from these figures we observe that stations farther away from the epicentre (like BFJ and KEF) experience longer duration shaking than those close to the epicentre.

This is because different wave phases emitted by the source and those generated along the propagation path get spread out in time as the epicentral distance increases.

From the recorded time series at KRY we observe that accelerations are higher in the E-W direction, especially during the earthquake of 24 February. However, ground velocity is higher in the N-S direction. This indicates that high- and low-frequency oscillations were polarized differently at this station.
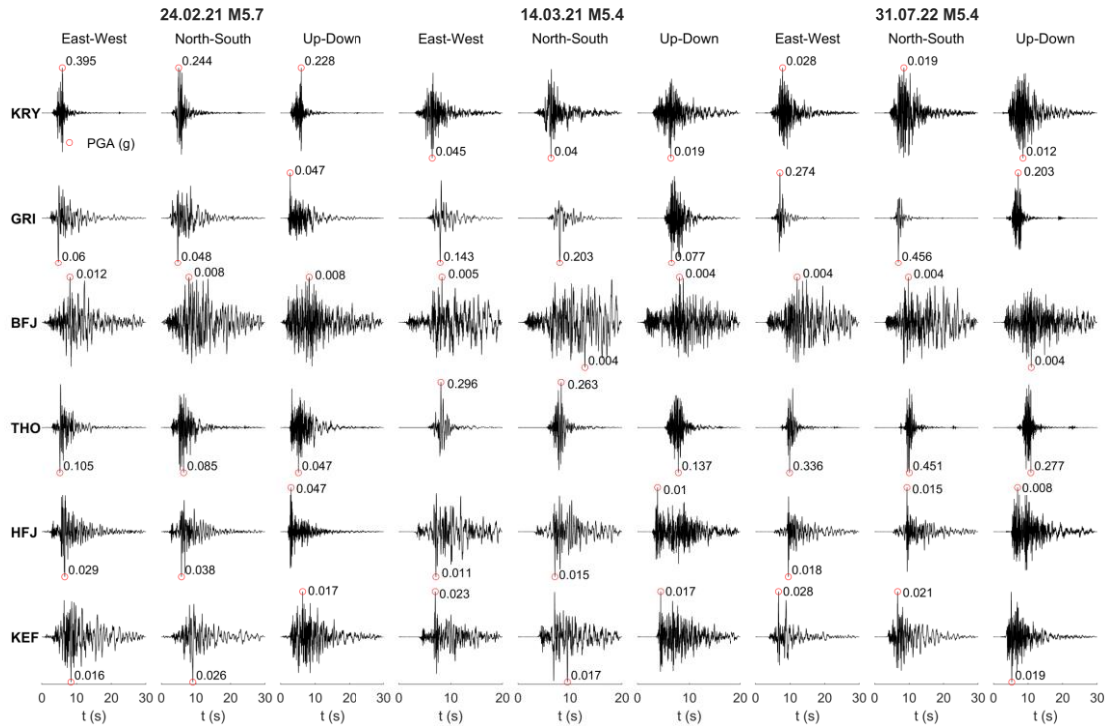

Fig. 5 Recorded acceleration seismograms at 6 stations of the IceSMN during the earthquakes of 24 February M5.7 (left), 14 March M5.4 (center), and 31 July M5.4 (right).
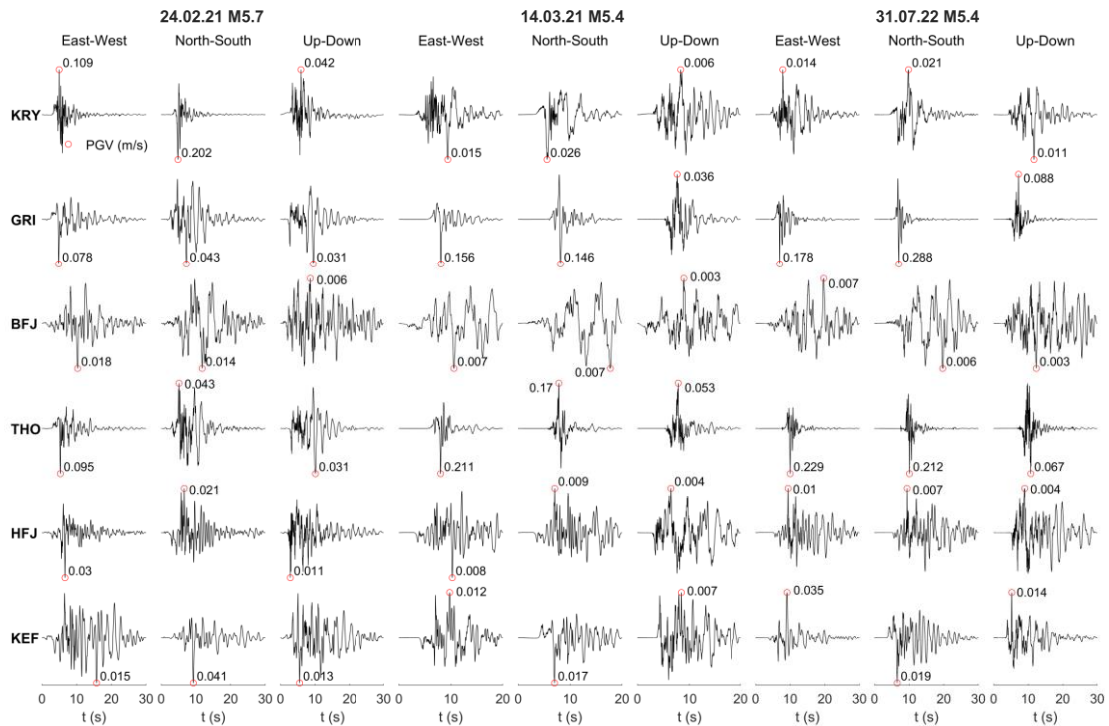
Fig. 6 Recorded ground velocity seismograms at 6 stations of the IceSMN during the earthquakes of 24 February M5.7 (left), 14 March M5.4 (center), and 31 July M5.4 (right).

Normalized Fourier amplitude spectra (FAS) for the event of 31 July 2022 and for the same set of stations as before are shown in Fig. 7. The evident low frequency content might be an indication that these volcano-tectonic events are of hybrid nature, as it will be discussed later.
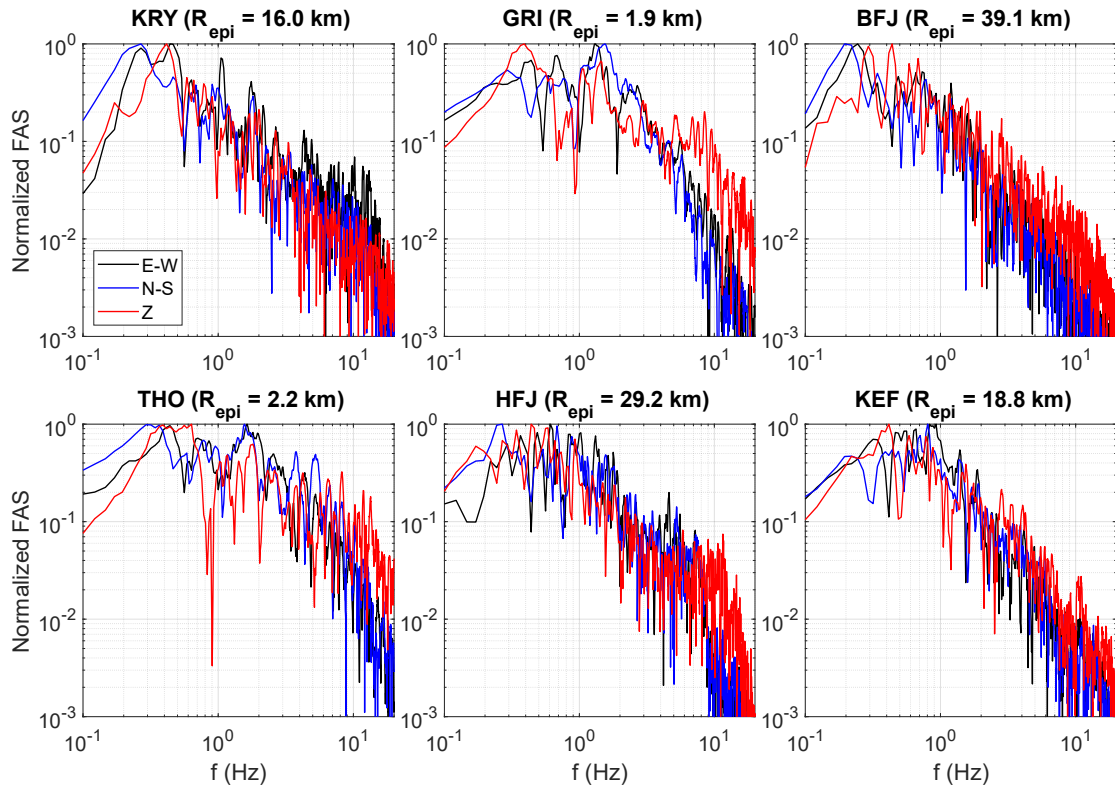

Fig. 7 Normalized Fourier amplitude spectra (FAS) of some of the recorded velocity waveforms during the 31 July 2022 M5.4 earthquake.

4.2 Elastic response spectra

Elastic response spectra (5% damped) of some of the recorded ground motions are presented in this section. In Fig. 8, Fig. 9, and Fig. 10 we show the acceleration response spectra of horizontal ground motion recorded at 6 stations of the IceSMN during the 24 February 2021 M5.7, 14 March 2021 M5.4, and 31 July 2022 M5.4 earthquakes, respectively. For comparison, 475-year return period Eurocode 8 Type 1 elastic spectrum for rock sites and corresponding to a PGA of 0.2g is also shown (SI, 2010). In all plots, the rotation-invariant response spectra, RotInv (Rupakhety & Sigbjörnsson, 2013), are also shown on the right. The rotation invariant spectra seem to lie near the middle of the east–west and the north–south spectra. Although the EC8 spectrum corresponds to 475-year return period and in that sense not directly comparable to a specific event, comparison between design ground motion and the actual shaking experienced by structures during an event is interesting from an engineering point of view, for example, to understand if structures have been exposed to shaking levels larger than they were designed to withstand.
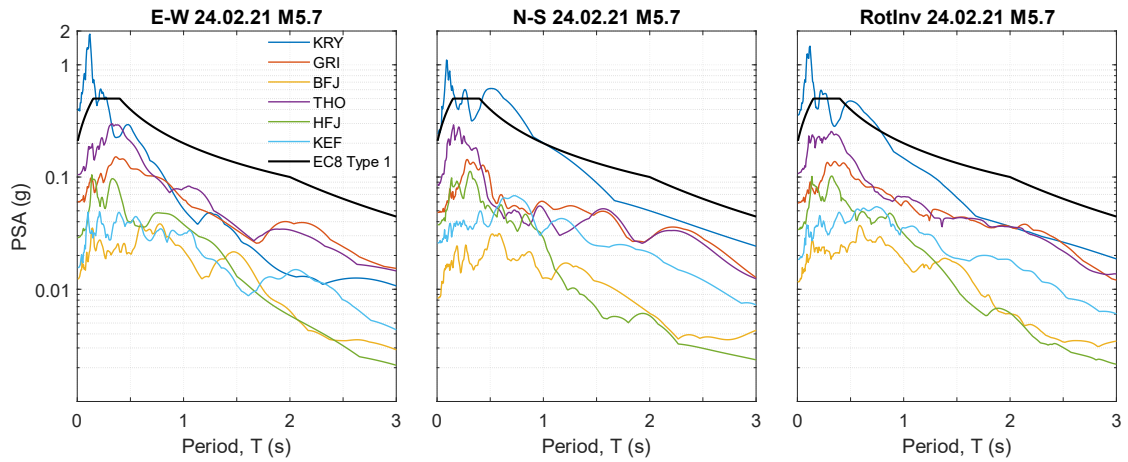
Fig. 8 Elastic pseudo-spectral accelerations (5% damping) of the horizontal ground motion recorded during the 24 February 2021 M5.7 earthquake at 6 stations of the IceSMN. RotInv stands for rotational-invariant.
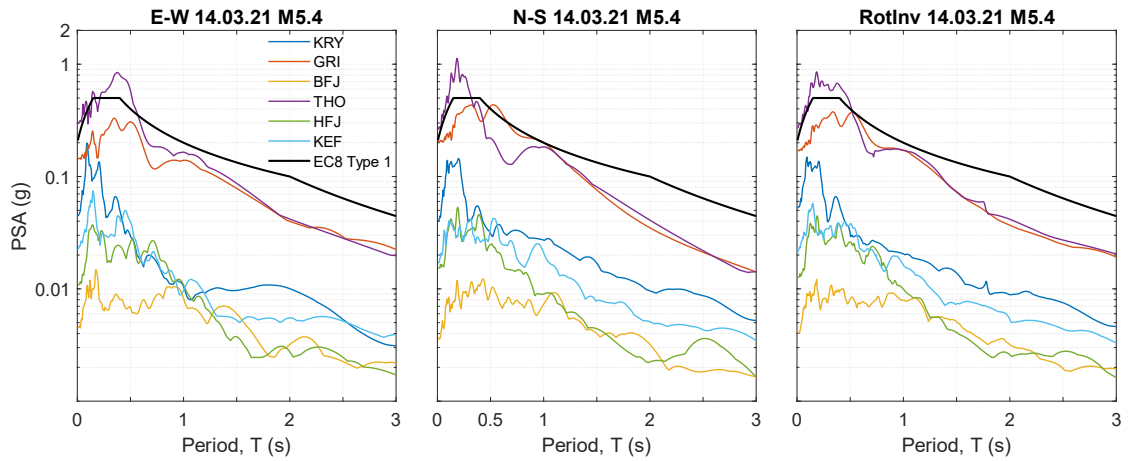

Fig. 9 Elastic pseudo-spectral accelerations (5% damping) of the horizontal ground motion recorded during the 14 March 2021 M5.4 earthquake at 6 stations of the IceSMN.
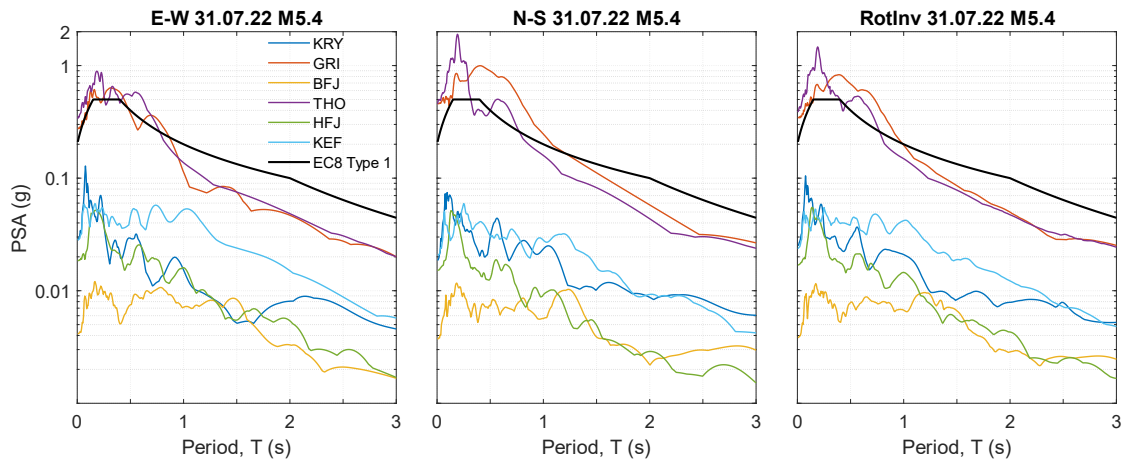

Fig. 10 Elastic pseudo-spectral accelerations (5% damping) of the horizontal ground motion recorded during the 31 July 2022 M5.4 earthquake at 6 stations of the IceSMN.

For the 24 February earthquake, the response spectra of recorded motion at Krýsuvík exceed the EC8 spectra, for vibration periods less than 0.2s, and also for periods of ~0.5s in the N-S component. This is the case even when the PGA of recorded motion is similar to the PGA used to scale the EC8 spectrum, for example the N-S component of recorded motion. Unusually high PGAs at KRY were recorded during various earthquakes, so we hypothesize that this station might be affected by site-effects. Detailed site characterization for this site is

not available, however, a geological map (Sæmundsson et al., 2016) for this area shows tephra deposits. Further geotechnical investigation is required to better understand local site effects at this station.

As mentioned before, although GRI and THO stations are very close to each other (see Fig. 1), their response spectra for both earthquakes are quite different in shape and amplitude. For low periods, the amplitudes at THO are larger than those at GRI in the E-W component. In the N-S component, there is a peak in the GRI spectrum at around T=0.5s. However, for lower periods, between 0.2s and 0.4s, the spectra at THO are twice as large as the spectra at GRI. The response spectra indicate that low rise buildings (2–4 stories) should have experienced the largest seismic demand.

We now focus on station Krýsuvík (KRY), where some of the largest PGAs and spectral accelerations were recorded. Fig. 11 shows the E-W, N-S and rotation-invariant acceleration response spectra at KRY for six earthquakes with M≥5. It is interesting to note that even earthquakes as small as M5.0 caused spectral accelerations larger than the 475-year EC8 design spectra. More interesting is the fact that design spectra was exceeded 3 times in just a one-week period, from 24 February 2021 to 1 March 2021. There are very few structures in the surroundings of Krýsuvík and no structural damage was reported in the area.
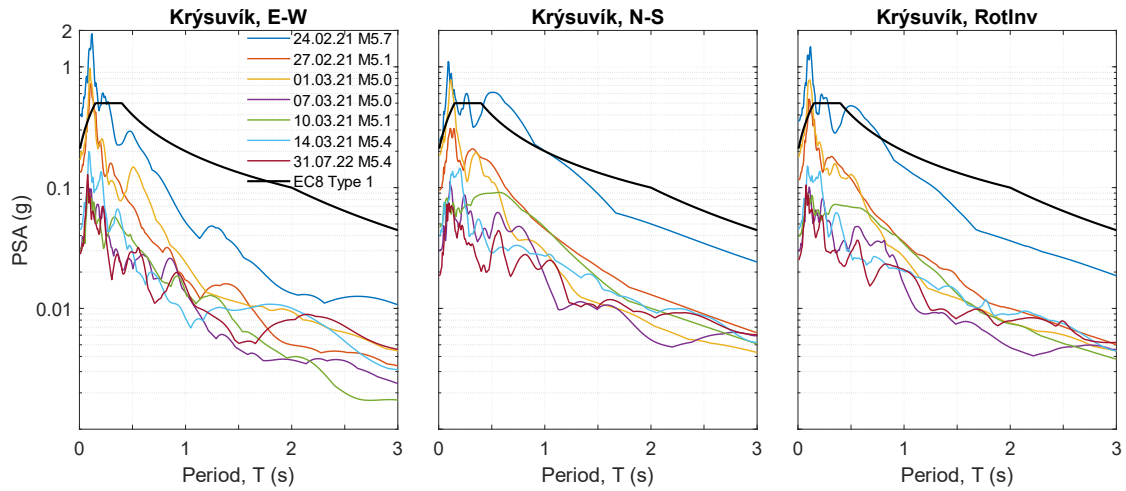

Fig. 11 Elastic pseudo-spectral accelerations (5% damping) of the horizontal ground motion recorded at Krýsuvík during six earthquakes with M≥5.

For the events of 24 and 27 February, the E-W spectral accelerations at KRY are much larger than spectral accelerations in the N-S direction at low periods. This could be related to polarization of ground motion close to the E-W direction. The polarization ellipses (e.g., Rupakhety & Sigbjörnsson, 2014) of the horizontal accelerations recorded at KRY are shown in Fig. 12. To compute the principal directions of ground motion (Penzien & Watabe, 1975), only the part of the time series between the 5% and 95% of the Arias intensity was considered. For the 27 February earthquake, the major principal direction is close to the E-W direction, explaining at least to some degree the contrast in the response spectra observed in Fig. 11. For the 1 March earthquake, we observe quite similar response spectra in the E-W and N-S directions, which is consistent with the polarization ellipsoid shown in Fig. 12. In general, the major principal direction appears to be close to the perpendicular to the epicentral direction (black arrow pointing towards the epicentre).
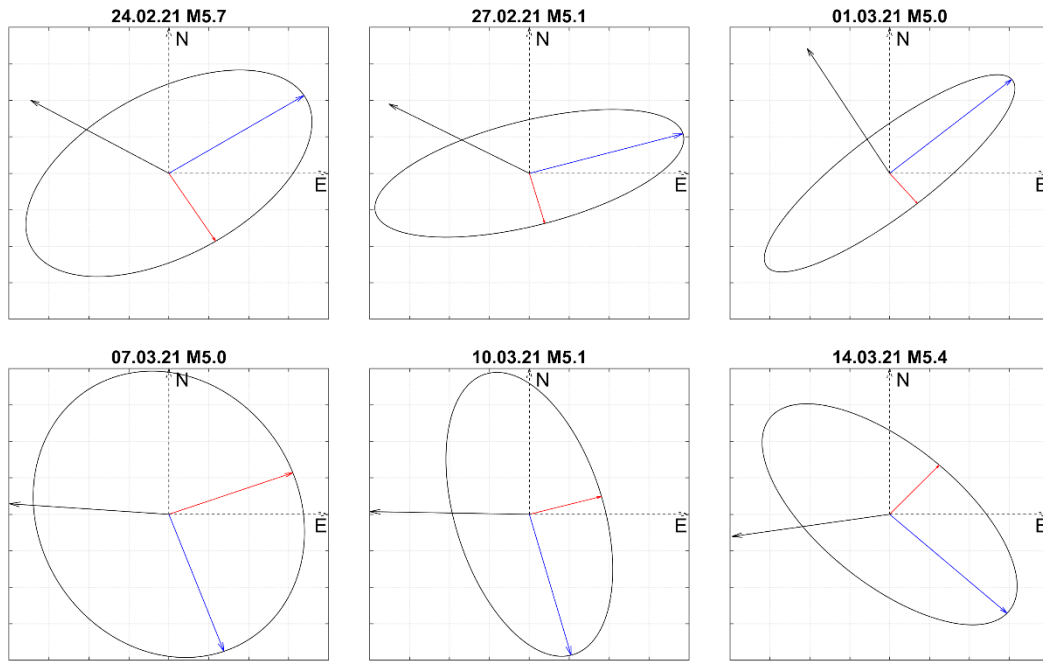
Fig. 12 Polarization ellipses and principal directions of horizontal ground acceleration recorded at Krýsuvík (KRY) during six earthquakes with M≥5.The blue and red arrows represent the major and minor principal directions, respectively, while the black arrow represents the epicentral direction.

The average of the normalized acceleration response spectra of the earthquakes with M≥5 for two stations, Keflavík (KEF) and GRI, are compared with the EC8 type 1 and type 2 spectral shapes for site class A in Fig. 13. For the horizontal direction, the rotation-invariant measure of the spectrum is used. We have selected these two stations because they are located in the two largest towns of the Peninsula. Overall, the EC8 type 1 spectral shape captures well the shape of the response spectra at both stations. The average normalized spectra recorded at GRI is included within the EC8 spectral shape, both horizontal and vertical, with a minor exception at around 0.2 s for the vertical component. Instead, at Keflavík, longer period components are present (beyond about 0.6 s and 0.25 s for the horizontal and vertical component, respectively) that make the recorded spectral shapes at such stations of unusual amplitude at long periods, also considering the low earthquake magnitude. Obviously, the difference of spectral shape would be even larger if the comparison were made with Type 2 EC8 spectra, that apply to countries with low seismicity.
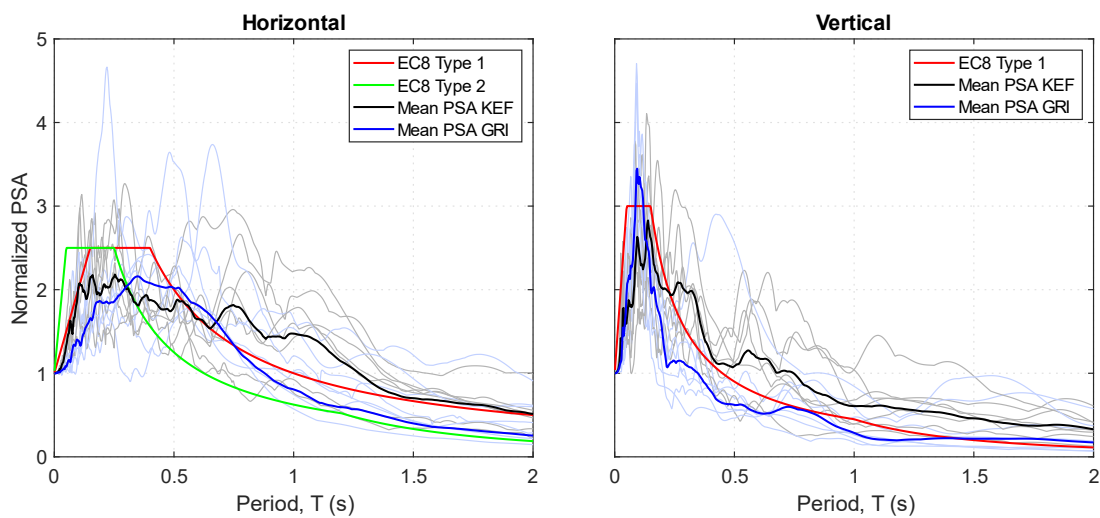

Fig. 13 Average of the normalized elastic pseudo-spectral response of acceleration (5% damping) compared with the Type 1(red) and Type 2 (green) EC8 site class A spectral shapes. The mean spectral shapes (thick lines) are computed from the spectra of the events with M≥5 (thin lines).

5 Ground-motion attenuation

Attenuations of the geometric mean of the horizontal (gmh) recorded PGA with epicentral distance (R_{epi}) for the three largest events of the swarm are shown in Fig. 14. Also shown are ground motion models (GMMs) of (1) Akkar et al. (2014), hereafter referred as Ak2014, that was derived based on data from tectonic earthquakes in Europe and the Middle East; and (2) Rupakhety et al. (2016), referred as Ru2016, which was calibrated from ground-motion data recorded from tectonic events in Iceland. Both models are presented for rock-site conditions, and a strike-slip faulting was used considering the focal mechanism in Table 1. In the figure, the solid curves represent the median values, and the dashed curves represent the mean values +/- one standard deviation. From Fig. 14 we observe that the Ru2016 model predicts lower peak ground accelerations, and fits the recorded data better than the Ak2014 model. It has previously been reported that GMMs calibrated from data outside Iceland, such as Ak2014, tend to underestimate ground motion at short distances and overestimate it further away from the source (e.g., Ólafsson & Sigbjörnsson, 2006).

Although the Ru2016 model seems to better capture the attenuation pattern of recorded horizontal PGA than the Ak2014 model, it appears to imply slower attenuation than what is observed from records. This is more evident for the M5.7 event. The model also tends to under-estimate PGA close to the epicentre, at R_{epi} less than about 10 km It is therefore interesting to interpret the recorded PGAs with observations from other global volcanic regions, as it will be made in the following.
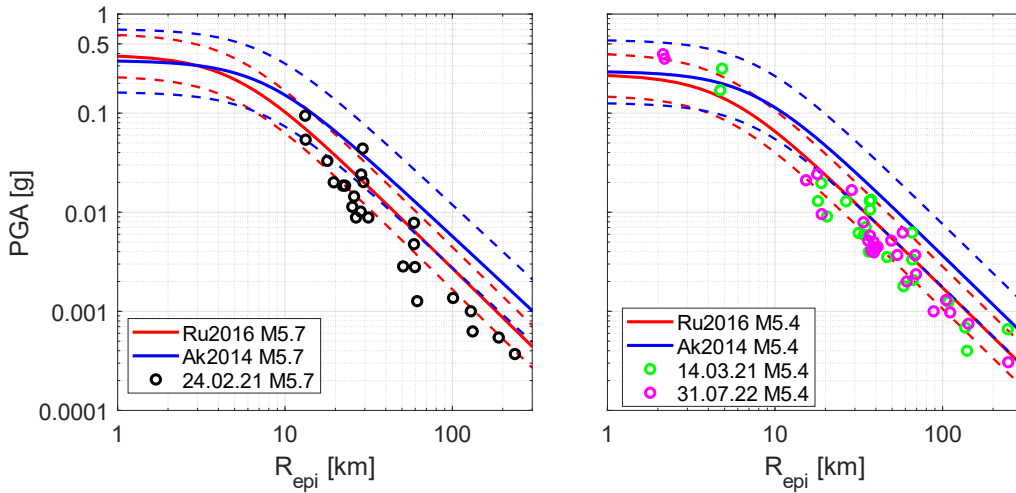

Fig. 14 Comparison of the GMPEs Ru2016 (red lines) and Ak2014 (blue lines) with the geometric mean of horizontal PGAs recorded by the IceSMN network during the 24.02.21 M5.7 (black circles), 14.03.21 M5.4 (green circles), and 31.07.22 M5.4 (magenta circles) earthquakes.

Volcanic earthquakes are mainly classified into three categories (see, for example, Lahr et al., 1994). The first category is the so-called Volcano-Tectonic (VT) or high-frequency earthquakes. Seismic signals from these earthquakes contain clear P and S-phases and contain significant energy at 5-15 Hz. They are usually a result of brittle failure and indistinguishable from double-couple tectonic earthquakes. The second category consists of the so-called Long-period (LP) earthquakes. These events are characterized by narrow-banded frequency content typically between 0.5 and 5 Hz. The origin of these events is often linked to movement of volcanic fluids. Finally, there is a hybrid type of volcanic events, which blends the characteristics of both VT and LP events. Tusa & Langer (2016) observe that ground motion characteristics at Mount Etna in Italy are different for events shallower and deeper than 5 km. They report that shallower events are like LP earthquakes with richer low-frequency content than deeper ones, while deeper events are similar to VT earthquakes with characteristics similar to tectonic earthquakes in active crustal regions. Further observations from volcanic earthquakes in Italy report that peak ground motion from volcanic events in Italy attenuate faster than typical shallow crustal tectonic events (Azzaro et al., 2006), that very close to the source volcanic events are associated with larger peak ground motion and high-frequency energy than typical tectonic events (Iervolino, 2018), and that hypocentral depth of volcanic earthquakes in Italy affects attenuation of peak ground motion, with deeper events showing slower attenuation at high-frequency than shallower events (Lanzano & Luzi, 2020). Based on these observations Lanzano and Luzi (2020) present a GMM for volcanic earthquakes in Italy, denoted hereafter by LL2020. Their model distinguishes between shallow and deep events by using different distance term. For shallow events, the geometric attenuation is only dependent on distance. For deep events (hypocentral depth larger than 5 km) they add an anelastic attenuation term in their model.

5.1 Ground motion model calibration

To calibrate a GMM for the recorded ground motions from the volcano-tectonic swarms in the Reykjanes Peninsula, consisting of 336 records from 22 earthquakes (Fig. 15), we adopt the functional form of LL2020 for shallow events, as follows

$$\log_{10}Y = a + b_1 M + c_1 \log_{10}\left(\sqrt{R_{hyp}^2 + h^2}\right) + \delta E_e + \delta S_s + \delta W_{0,es} \qquad (1)$$

where Y is the observed intensity measure (IM), a is the offset, M is the magnitude, R_{hyp} is the hypocentral distance, the pseudo-depth is h= 5 km. In this linear mixed-effects model, the coefficients a, b_1, and c_1 represent the fixed part, while δE_e and δS_s represent between event and site-to-site random effects modelled as Gaussian random variables with 0 mean and standard deviations τ and ϕ_s, respectively. The event- and site-corrected residual is represented by $\delta W_{0,es}$, which is modelled as a Gaussian random variable with 0 mean and standard deviation σ_0. The total standard deviation of the model is obtained as

$$\sigma_T = \sqrt{\tau^2 + \phi_s^2 + \sigma_0^2} \qquad (2)$$
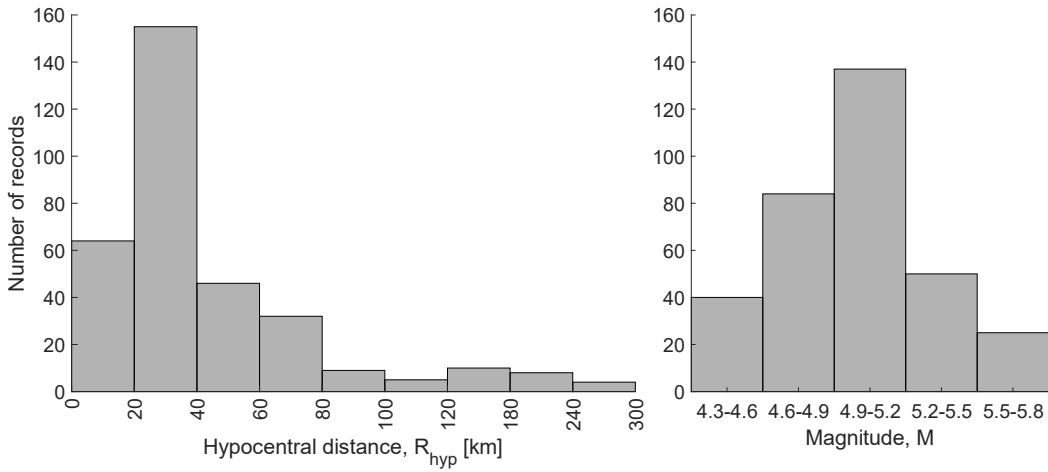

Fig. 15 Distribution of the records as a function of the hypocentral distance (left), and magnitude (right).

Since station KRY might have been affected by site effects, as mentioned before, we did not include this station for the calibration of the GMM model. We do not include a quadratic term for magnitude dependence since we observed a linear dependence of PGA and PSA on magnitude from our data, evident in Fig. 16. This term is usually used to represent the saturation of ground motion observed for large magnitudes, however, most likely because of the relatively low magnitudes of our dataset, we do not observe this saturation. Furthermore, from preliminary nonlinear regressions we obtained low "pseudo-depth" h values (<2). This parameter has the effect of introducing a saturation of ground motion at small distances from the source, and for shallow sources, as the ones we are considering, it mirrors the effect of source extension rather than depth (Tusa et al., 2020). Keeping this in mind and considering the magnitude range of the events in our dataset, and their corresponding small source extensions, we fixed h=5 km.
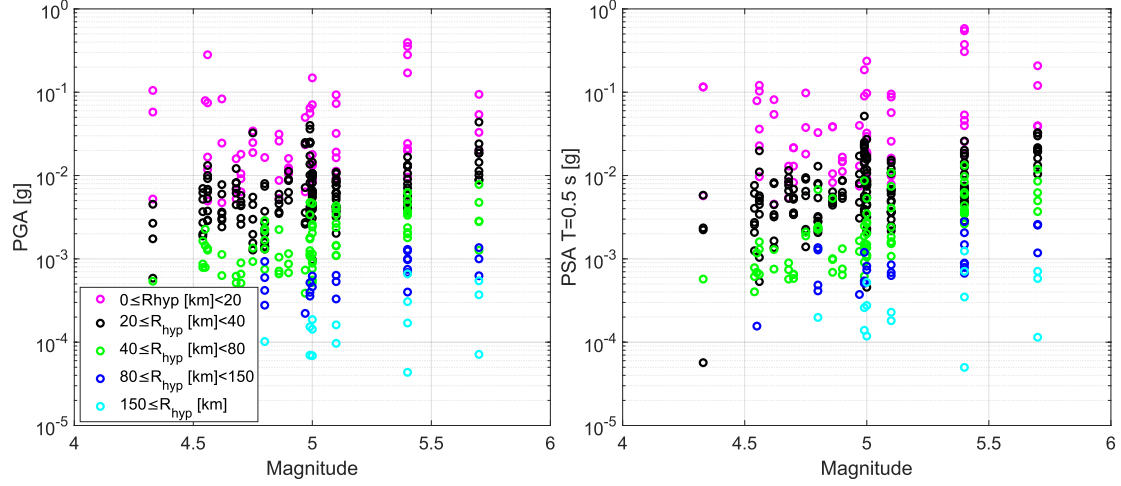
Fig. 16 PGA versus magnitude for different distance classes (left), and PSA amplitudes at T = 0.5 s versus magnitude for different distance classes (right).

The resulting model, hereafter called as HR2023, is calibrated for the geometric mean of the horizontal components of PGA (m/s^2), PGV (m/s) and 24 ordinates of PSA (from T = 0.04 s to T = 5 s) for rock sites (EC8 site category A). Since all the considered earthquakes are shallow, we do not separate the dataset in different depth classes. The coefficients of the regression are presented in Table 3. The magnitude scaling parameter is b_1=0.44591 for PGA, which is smaller than b_1 for other GMMs for small earthquakes, that have b_1 of around 0.8 (e.g., Lanzano & Luzi, 2020; Massa et al., 2007). In LL2020, the larger b_1 seems to be driven by the records at large distances, that are the majority in their dataset, since these show a larger increase of ground motion amplitude with magnitude than near-field records (see their Fig. 4). From our Fig. 16 this trend is not observed.

Table 3 Coefficients of the predictive model for volcanic events (HR2023) given by Equation (1) for peak ground acceleration (PGA), peak ground velocity (PGV) and spectral accelerations (PSA), for the geometric mean of the horizontal components.

IM	a	b_1	c_1	τ	ϕ_s	σ_0	σ_T
PGA	-0.27645	0.44591	-2.13139	0.11476	0.16947	0.19223	0.28079
PGV	-2.95308	0.71704	-1.98977	0.10862	0.25552	0.16593	0.32346
PSA T=0.04 s	-0.10278	0.41840	-2.08303	0.10711	0.15834	0.20848	0.28286
PSA T=0.07 s	0.22041	0.40975	-2.20134	0.11220	0.16714	0.20705	0.28878
PSA T=0.1 s	0.29626	0.40850	-2.21442	0.12210	0.18341	0.20806	0.30305
PSA T=0.15 s	0.14248	0.44414	-2.20832	0.11773	0.17223	0.22218	0.30477
PSA T=0.2 s	0.33523	0.39365	-2.16829	0.12553	0.20055	0.21638	0.32062
PSA T=0.25 s	-0.08494	0.46758	-2.15172	0.13815	0.22627	0.22506	0.34776
PSA T=0.3 s	-0.53740	0.54865	-2.14315	0.13834	0.22432	0.22719	0.34796
PSA T=0.4 s	-1.06954	0.61220	-2.07104	0.12691	0.20656	0.22139	0.32831
PSA T=0.5 s	-1.37276	0.66818	-2.09918	0.13236	0.20164	0.21380	0.32232
PSA T=0.6 s	-1.74413	0.67886	-1.92805	0.11278	0.23157	0.20814	0.33116
PSA T=0.7 s	-1.87035	0.68428	-1.87464	0.09742	0.25142	0.20984	0.34167
PSA T=0.8 s	-2.11051	0.71198	-1.82839	0.09729	0.28185	0.20349	0.36099
PSA T=1.0 s	-2.78841	0.76965	-1.65447	0.10396	0.27083	0.19857	0.35155
PSA T=1.2 s	-3.13283	0.80589	-1.60804	0.10929	0.27299	0.20583	0.35893
PSA T=1.4 s	-3.38336	0.82466	-1.56943	0.09319	0.25779	0.20166	0.34030
PSA T=1.7 s	-3.71103	0.83169	-1.46180	0.11358	0.23030	0.19834	0.32446
PSA T=2.0 s	-4.12366	0.87665	-1.41495	0.12531	0.24051	0.19461	0.33379
PSA T=2.5 s	-4.32715	0.89222	-1.42700	0.14781	0.25241	0.19817	0.35331
PSA T=3.0 s	-4.60689	0.91323	-1.38580	0.15777	0.30118	0.19701	0.39295
PSA T=4.0 s	-5.10093	0.96001	-1.32657	0.16421	0.36446	0.21439	0.45361

In Fig. 17 we compare the attenuation of the recorded gmh PGA for three magnitude ranges with the LL2020, HR2023 and Ru2016 models. LL2020 is computed for shallow events. Both the LL2020 and HR2023 models predict higher PGA close to the source (epicentral distance lower than 10 km) than the Ru2016 model, which is mostly based on tectonic events recorded in Iceland. For the lowest magnitude range, M 4.5-4.7, LL2020 underpredicts all the recorded data. Although the LL2020 model is strictly valid up to M 5.0 only, extrapolation to fit the recordings from M 5.7 provides satisfactory results, at least for distances larger than 10 km that is where we have data. At this magnitude, it predicts higher PGA than the HR2023 model at closer distances (<10 km). Combined with the observation that LL2020 under-predicts PGA of smaller magnitude events at closer distances, this exhibits the different magnitude scaling (b_1 coefficient) in the HR2023 and LL2020 models mentioned before, although their attenuation rates are similar. The different magnitude scaling of HR2023 and LL2020 is also evident from the last figure in the Online Resource 1 (ESM_1), where PSA for three magnitude ranges are plotted. Additional plots, comparing recorded PSA with HR2023 for T=0.2 s, 0.5 s and 1 s, are available in the Online Resource 1.
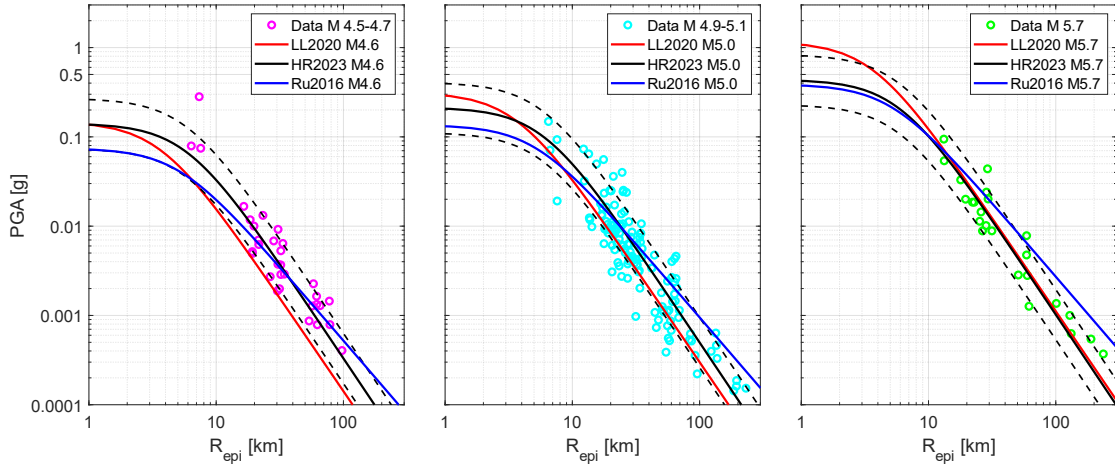

Fig. 17 Comparison of the GMMs LL2020 for shallow events (red lines), Ru2016 (blue lines), and HR2023 (black lines) with the geometric mean of horizontal peak ground accelerations recorded by the IceSMN network during the 2021 and 2022 swarms in the Reykjanes Peninsula for three magnitude ranges. R_{epi} is computed from R_{hyp} with depth=3 km.

Overall, the recorded data clearly shows that the ground motion from volcanic events in the Reykjanes Peninsula attenuates much faster than that from tectonic events recorded in the past in Iceland. Due to the relatively large magnitude of these events, one would expect them to be similar to VT earthquakes (i.e., caused by brittle failure). The recorded waveforms (Fig. 6) show a rich long-period energy content, evident from the Fourier amplitude spectra (FAS) presented in Fig. 7, with higher frequencies during the first few seconds, characteristic of hybrid events according to Lahr et al. (1994). Therefore, the ground motion model presented here is valid for VT and hybrid earthquakes, and it should be used with care in volcanic zones that present earthquakes of different characteristics.

The total sigma for PGA is σ_T=0.2808, which is relatively low when compared to some GMMs, such as LL2020 for which for PGA σ_T=0.392. However, low sigma values are commonly obtained for GMMs calibrated with datasets including recordings from Iceland (e.g., Kowsari et al., 2019; Rupakhety & Sigbjörnsson, 2009). A low sigma was expected since we used records from the same region and the considered earthquakes were of similar characteristics. We expect that our sigma values will increase when more observations, particularly from other volcanic regions in Iceland, will become available.

The epistemic uncertainty is provided for the use of the GMM in logic trees in probabilistic seismic hazard assessment. The epistemic uncertainty can be partially quantified by estimating the statistical uncertainty in the median predictions, calculated on the model fit and the data distribution. For a set of predictor variables (location x_0), the epistemic uncertainty can be calculated as (Al Atik & Youngs, 2014; Bindi et al., 2017):

$$\sigma_\mu = \sqrt{J_0^T [varCOV_{x_i}] J_0} \tag{3}$$

in which x_i are the data points used to develop the model; J_0 is the Jacobian matrix, i.e, the gradient of the model with respect to its coefficients, evaluated in the predictive location x_0; and varCov$_{xi}$ is the variance–covariance matrix of the coefficients, evaluated at all data points x_i. σ_μ quantifies the epistemic uncertainty due to the combined effects of limited data availability and implemented functional form. **Fig. 18** shows σ_μ for

different magnitude and distance scenarios. σ_μ is strongly dependent on magnitude, as already observed by other authors (e.g., Bindi et al., 2017; Lanzano & Luzi, 2020, with larger values are at the extremes of the validity range. Moreover, σ_μ is larger at short distances, mainly due to the limited amount of data available for the model calibration.
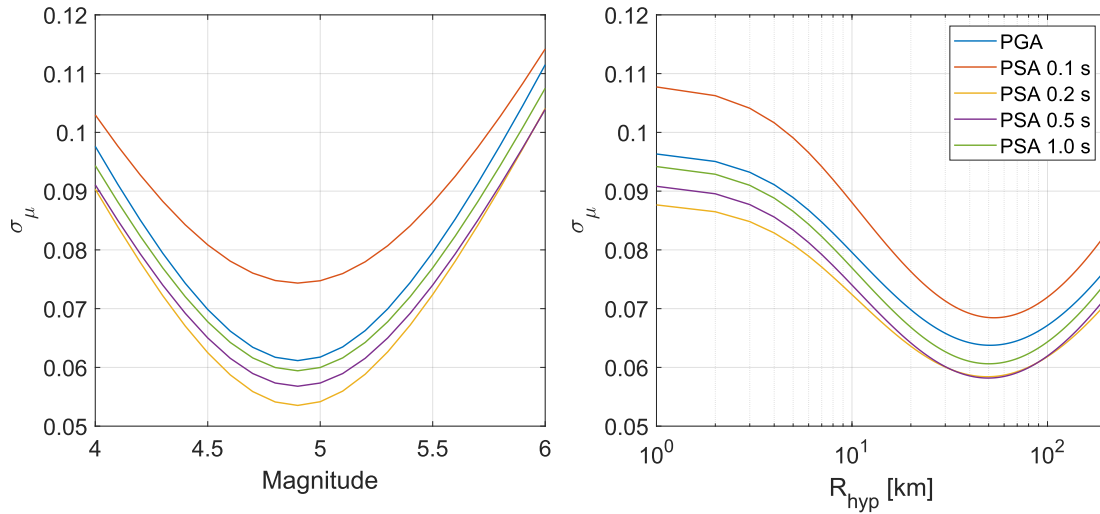

Fig. 18 Epistemic uncertainty σ_μ as a function of magnitude (R_{hyp}=10 km) and hypocentral distance R_{hyp} (M=5.5).

6 Conclusions

This work presents a general overview of the seismicity on the Reykjanes Peninsula from January 2020 to August 2022. The seismicity in Fagradalsfjall prior to the 2021 eruption formed two clusters close to the eruption sites. The NE-SW trending cluster maps the dyke propagation, while the WSW-ENE trending cluster follows the plate boundary. The swarm started at its north-east end, then migrated south-westward, and finally, the seismicity jumped back to the central part where the Geldingadalir effusive eruption eventually occurred on March 19th. The eruption lasted for six months. From 24 February 2021 to 19 March 2021, ~4000 earthquakes with M>1 were reported in Fagradalsfjall. Just minor non-structural damages were reported during this swarm.

The unrest on the Peninsula continued after the first eruption. On December 2021 a new swarm occurred, with the largest earthquake having a M4.8, followed by another swarm on 30 July 2022, preceding the Meradalir eruption of 3 August 2022, with 358 earthquakes of M>1 reported by IMO from 30 July 2022 to the start of the eruption. The largest event of this swarm was a M5.4, after which rock falls, pipeline breakage, and non-structural damages were reported.

A total of eight earthquakes had a magnitude M>5 in the Reykjanes Peninsula from January 2020 to August 2022, mostly with a N-S right-lateral strike-slip faulting. During this period there were 92 events with M>4, while for the same area there were just 13 events of M>4 from 2000 to 2020 (Jónasson et al., 2021). The seismic activity on the peninsula is not uniform in time and in periods with volcanic activity the frequency of larger events, that can affect the built environment, are considerable higher than in periods when seismic activity is controlled by tectonic events. This must be considered in probabilistic seismic hazard analyses for the area.

During the 31 July 2022 M5.4 earthquake, the largest PGA was recorded with ~0.45g at Grindavík (GRI), which is more than twice the 475-year return period PGA of 0.2g for the area (SI, 2010). During the largest event of the swarms, the 24 February 2021 M5.7 earthquake, a PGA of ~0.4g was recorded at Krýsuvík (KRY). Site-effects at Krýsuvík are a plausible explanation for the unusually large PGAs and high spectral accelerations at short periods, although further geotechnical investigation is required to better understand local site effects at this station.

Ground motion at the nearby stations were, in general, anisotropic, and polarized roughly perpendicular to the epicentral direction. The elastic response spectral shapes of ground motion recorded at nearby stations show unusually broad-band plateau and large amplitudes at long periods. As a result, the spectral shapes are more consistent with EC8 Type 1 spectra than the Type 2 spectra, which is unusual for earthquake of such small size. This is an indication of ground shaking rich in low-frequency components, which is evident from the recorded waveforms and from the FAS presented in Fig. 7. The FAS also show some energy content at higher frequencies, and because of the relatively large magnitude of the earthquakes considered here, these events

were caused by brittle failure (VT earthquakes) but exhibit some characteristics of LP earthquakes, hence, the events presented here are most likely hybrid volcanic earthquakes.

The attenuation of ground motion with distance is faster than what has been observed from past records of tectonic earthquakes in Iceland. It is interesting to note that attenuation of tectonic events in Iceland is found to be faster than similar events in Europe and the Middle East, and the data presented here show even faster attenuation for earthquakes of volcanic origin. Peak ground motion near the source is higher, on the average, than the tectonic-type empirical GMPEs developed for Iceland. This is consistent with observations from Italy that volcanic events produce larger peak motion than tectonic events very close to the source (Iervolino, 2018). A mixed-effects empirical ground motion model was developed for the horizontal (gmh) PGA, PGV as well as PSA, referred as HR2023, using the same functional form as that of LL2020, in order to highlight clearly the different trends of our dataset with respect to that used by LL2020.

The distance attenuation coefficient (c_1) of both models is similar. As shown in Fig. 17, and also made evident by the different b_1 parameters in Eq. 1, there is a different dependence on magnitude of the two models, with LL2020 underestimating recorded PGAs for M smaller than about 4.7, while in good agreement with records for M5. For M5.7, both models predict very similar PGA values for distances larger than 10 km (even though M>5 fall outside the calibration range of LL2020), while LL2020 predicts higher PGA than HR2023 at lower distances. For instance, for M5.7 at R_{hyp}=3 km, LL2020 predicts a PGA of ~1g, which is around two times larger than PGA predicted by HR2023. The ground motion in this magnitude and distance range is of outmost importance for seismic hazard studies and the use of either GMM would give very different results.

The overall results indicate that scaling and attenuation of ground motion from volcanic events and purely tectonic earthquakes in Iceland are different with respect to those considered in LL2020 for Italian volcanic earthquakes. This is an important observation because seismic hazard in parts of the Reykjavik and surrounding area could potentially be dominated by events of volcanic origin. This is also the case for certain parts of the highlands close to volcanic systems, where important infrastructure of hydroelectric power plants are located. It is therefore considered important to take these observations into account for ground motion modelling in seismic hazard and risk assessment in Iceland.

Declarations

Conflict of interest R Paolucci declares to be an associated editor. The rest of the authors declare no competing interests.

References

Aki, K. (1965). Maximum likelihood estimate of b in the formula log N=a-bM and its confidence limits. *Bulletin of the Earthquake Research Institute*, *43*, 237–239.

Akkar, S., Sandıkkaya, M. A., & Bommer, J. J. (2014). Empirical ground-motion models for point- and extended-source crustal earthquake scenarios in Europe and the Middle East. *Bulletin of Earthquake Engineering*, *12*(1), 359–387. https://doi.org/10.1007/s10518-013-9461-4

Al Atik, L., & Youngs, R. R. (2014). Epistemic uncertainty for NGA-West2 models. *Earthquake Spectra*, *30*(3), 1301–1318. https://doi.org/10.1193/062813EQS173M

Árnadóttir, T., Geirsson, H., & Einarsson, P. (2004). Coseismic stress changes and crustal deformation on the Reykjanes Peninsula due to triggered earthquakes on 17 June 2000. *Journal of Geophysical Research: Solid Earth*, *109*. https://doi.org/10.1029/2004JB003130

Azzaro, R., Barbano, M. S., D'Amico, S., & Tuvè, T. (2006). The attenuation of seismic intensity in the Etna region and comparison with other Italian volcanic districts. *Annals of Geophysics*, *49*(4–5), 1003–1020. https://doi.org/10.4401/ag-3113

Bindi, D., Cotton, F., Kotha, S. R., Bosse, C., Stromeyer, D., & Grünthal, G. (2017). Application-driven ground motion prediction equation for seismic hazard assessments in non-cratonic moderate-seismicity areas. *Journal of Seismology*, *21*(5), 1201–1218. https://doi.org/10.1007/s10950-017-9661-5

Björnsson, S., Einarsson, P., Tulinius, H., & Hjartardóttir, Á. R. (2020). Seismicity of the Reykjanes Peninsula 1971–1976. *Journal of Volcanology and Geothermal Research*, *391*, 106369. https://doi.org/10.1016/j.jvolgeores.2018.04.026

Böðvarsson, R., Rögnvaldsson, S., Jakobsdóttir, S. S., Slunga, R., & Stefánsson, R. (1996). The SIL Data Acquisition and Monitoring System. *Seismological Research Letters*, *67*(5), 35–46.

Böðvarsson, R., Rögnvaldsson, S., Slunga, R., & Kjartansson, E. (1999). The SIL data acquisition system-at present and beyond year 2000. *Physics of the Earth and Planetary Interiors*, *113*, 89–101.

Clifton, A. E., & Kattenhorn, S. A. (2006). Structural architecture of a highly oblique divergent plate boundary segment. *Tectonophysics*, *419*(1–4), 27–40. https://doi.org/10.1016/j.tecto.2006.03.016

DeMets, C., Gordon, R. G., & Argus, D. F. (2010). Geologically current plate motions. *Geophysical Journal International*, *181*(1), 1–80. https://doi.org/10.1111/j.1365-246X.2009.04491.x

Dziewonski, A. M., Chou, T.-A., & Woodhouse, J. H. (1981). Determination of earthquake source parameters from waveform data for studies of global and regional seismicity. *Journal of Geophysical Research: Solid Earth*, *86*(B4), 2825–2852. https://doi.org/10.1029/JB086iB04p02825

Einarsson, P. (1991). Earthquakes and present-day tectonism in Iceland. *Tectonophysics*, *189*(1–4), 261–279. https://doi.org/10.1016/0040-1951(91)90501-I

Einarsson, P. (2008). Plate boundaries, rifts and transforms in Iceland. *Jokull*, *58*, 35–58.

Einarsson, P., Bjornsson, S., Foulger, G., Stefansson, R., & Skaftadottir, T. (1981). Seismicity pattern in the South Iceland Seismic Zone. *In Earthquake Prediction (Eds D.W. Simpson and P.G. Richards)*, *March 2016*, 141–151. https://doi.org/10.1029/me004p0141

Ekström, G., Nettles, M., & Dziewoński, A. M. (2012). The global CMT project 2004–2010: Centroid-moment tensors for 13,017 earthquakes. *Physics of the Earth and Planetary Interiors*, *200–201*, 1–9. https://doi.org/10.1016/j.pepi.2012.04.002

Fischer, T., Hrubcová, P., Salama, A., Doubravová, J., Ágústsdóttir, T., Gudnason, E., Horálek, J., & Hersir, G. P. (2022). Swarm seismicity illuminates stress transfer prior to the 2021 Fagradalsfjall eruption in Iceland. *Earth and Planetary Science Letters*, *594*. https://doi.org/10.1016/j.epsl.2022.117685

Flóvenz, Ó. G., Wang, R., Hersir, G. P., Dahm, T., Hainzl, S., Vassileva, M., Drouin, V., Heimann, S., Isken, M. P., Gudnason, E. Á., Ágústsson, K., Ágústsdóttir, T., Horálek, J., Motagh, M., Walter, T. R., Rivalta, E., Jousset, P., Krawczyk, C. M., & Milkereit, C. (2022). Cyclical geothermal unrest as a precursor to Iceland's 2021 Fagradalsfjall eruption. *Nature Geoscience*, *15*(5), 397–404. https://doi.org/10.1038/s41561-022-00930-5

Geirsson, H., Parks, M., Vogfjörd, K., Einarsson, P., Sigmundsson, F., Jónsdóttir, K., Drouin, V., Ófeigsson, B. G., Hreinsdóttir, S., Ducrocq, C., Geirsson, H., Parks, M., Vogfjörd, K., Einarsson, P., Sigmundsson, F., Jónsdóttir, K., Drouin, V., Ófeigsson, B. G., Hreinsdóttir, S., & Ducrocq, C. (2021). The 2020 volcano-tectonic unrest at Reykjanes Peninsula, Iceland: stress triggering and reactivation of several volcanic systems. *EGU General Assembly 2021, Online, 19–30 Apr 2021*, EGU21-7534. https://doi.org/https://doi.org/10.5194/egusphere-egu21-7534, 2021

Gutenberg, B., & Richter, C. F. (1944). Frequency of earthquakes in California. *Bulletin of the Seismological Society of America*, *34*(4), 185–188. https://doi.org/10.1785/BSSA0340040185

Hreinsdóttir, S., Einarsson, P., & Sigmundsson, F. (2001). Crustal deformation at the oblique spreading Reykjanes Peninsula, SW Iceland: GPS measurements from 1993 to 1998. *Journal of Geophysical Research: Solid Earth*, *106*(B7), 13803–13816. https://doi.org/10.1029/2001jb000428

Hrubcová, P., Doubravová, J., & Vavryčuk, V. (2021). Non-double-couple earthquakes in 2017 swarm in Reykjanes Peninsula, SW Iceland: Sensitive indicator of volcano-tectonic movements at slow-spreading rift. *Earth and Planetary Science Letters*, *563*. https://doi.org/10.1016/j.epsl.2021.116875

Iervolino, I. (2018). Il moto al suolo nel terremoto di Viagrande. *Progettazione Sismica*, *3*(in Italian), 5–8. https://doi.org/10.1007/s10518-018-00531-x

IMO. (2022a). *Earthquake Catalogue*. Icelandic Meteorological Office. http://hraun.vedur.is/ja/viku/.

IMO. (2022b). *https://www.vedur.is/um-vi/frettir/jardskjalftahrina-a-reykjanesi*. accessed 20 November 2022.

Jóhannesson, H., & Sæmundsson, K. (2009). *Geological Map of Iceland, 1:600 000, Tectonics*. Icelandic Institute of Natural History.

Jónasson, K., Bessason, B., Helgadóttir, Á., Einarsson, P., Guðmundsson, G. B., Brandsdóttir, B., Vogfjörd, K. S., & Jónsdóttir, K. (2021). A harmonised instrumental earthquake catalogue for Iceland and the northern Mid-

Atlantic Ridge. *Natural Hazards and Earth System Sciences*, *21*(7), 2197–2214. https://doi.org/10.5194/nhess-21-2197-2021

Keiding, M., Lund, B., & Árnadóttir, T. (2009). Earthquakes, stress, and strain along an obliquely divergent plate boundary: Reykjanes Peninsula, southwest Iceland. *Journal of Geophysical Research: Solid Earth*, *114*(9), 1–16. https://doi.org/10.1029/2008JB006253

Kowsari, M., Halldorsson, B., Hrafnkelsson, B., Snæbjörnsson, J. Þ., & Jónsson, S. (2019). Calibration of ground motion models to Icelandic peak ground acceleration data using Bayesian Markov Chain Monte Carlo simulation. *Bulletin of Earthquake Engineering*, *17*(6), 2841–2870. https://doi.org/10.1007/s10518-019-00569-5

Lahr, J. C., Chouet, B. A., Stephens, C. D., Power, J. A., & Page, R. A. (1994). Earthquake classification, location, and error analysis in a volcanic environment: implications for the magmatic system of the 1989-1990 eruptions at Redoubt Volcano, Alaska. In *Journal of Volcanology and Geothermal Research* (Vol. 62).

Lanzano, G., & Luzi, L. (2020). A ground motion model for volcanic areas in Italy. *Bulletin of Earthquake Engineering*, *18*(1), 57–76. https://doi.org/10.1007/s10518-019-00735-9

Massa, M., Marzorati, S., D'Alema, E., Di Giacomo, D., & Augliera, P. (2007). Site classification assessment for estimating empirical attenuation relationships for Central-Northern Italy earthquakes. *Journal of Earthquake Engineering*, *11*(6), 943–967. https://doi.org/10.1080/13632460701232675

Ólafsson, S., & Sigbjörnsson, R. (2006). Attenuation in Iceland compared with other regions. *First European Conference on Earthquake Engineering and Seismology (1ECEES)*, *September*, Paper no. 1157.

Panzera, F., Zechar, J. D., Vogfjörd, K. S., & Eberhard, D. A. J. (2016). A Revised Earthquake Catalogue for South Iceland. *Pure and Applied Geophysics*, *173*(1), 97–116. https://doi.org/10.1007/s00024-015-1115-9

Pedersen, G. B. M., Belart, J. M. C., Óskarsson, B. V., Gudmundsson, M. T., Gies, N., Högnadóttir, T., Hjartardóttir, Á. R., Pinel, V., Berthier, E., Dürig, T., Reynolds, H. I., Hamilton, C. W., Valsson, G., Einarsson, P., Ben-Yehosua, D., Gunnarsson, A., & Oddsson, B. (2022). Volume, Effusion Rate, and Lava Transport During the 2021 Fagradalsfjall Eruption: Results From Near Real-Time Photogrammetric Monitoring. *Geophysical Research Letters*, *49*(13). https://doi.org/10.1029/2021GL097125

Penzien, J., & Watabe, M. (1975). Characteristics of 3-dimensional earthquake ground motions. *Earthquake Engineering & Structural Dynamics*, *3*(4), 365–373. https://doi.org/10.1002/eqe.4290030407

Pétursson, G. G., & Vogfjörð, K. S. (2009). *Attenuation relations for near-and far-field peak ground motion (PGV, PGA) and new magnitude estimates for large earthquakes in SW-Iceland*. Icelandic Meteorological. Report no VI 2009-012, ISSN 1670-8261.

Ramadan, F., Smerzini, C., Lanzano, G., & Pacor, F. (2021). An empirical model for the vertical-to-horizontal spectral ratios for Italy. *Earthquake Engineering and Structural Dynamics*, *50*(15), 4121–4141. https://doi.org/10.1002/eqe.3548

Rögnvaldsson, S. Th., & Slunga, R. (1993). Routine fault plane solutions for local networks: A test with synthetic data. *Bulletin of the Seismological Society of America*, *83*(4), 1232–1247. https://doi.org/10.1785/BSSA0830041232

Rupakhety, R., Ólafsson, S., & Sigurðsson, G. (2016). Site response analysis and near-fault effects for seismic resistant design of wind turbine towers in the Búrfellslundur area. *Landsvirkjun Report Number LV-2016-040*.

Rupakhety, R., & Sigbjörnsson, R. (2009). Ground-motion prediction equations (GMPEs) for inelastic response and structural behaviour factors. *Bulletin of Earthquake Engineering*, *7*(3), 637–659. https://doi.org/10.1007/s10518-009-9105-x

Rupakhety, R., & Sigbjörnsson, R. (2013). Rotation-invariant measures of earthquake response spectra. *Bulletin of Earthquake Engineering*, *11*(6), 1885–1893. https://doi.org/10.1007/s10518-013-9472-1

Rupakhety, R., & Sigbjörnsson, R. (2014). Three-Dimensional Characteristics of Strong Ground Motion in the Near-Fault Area. *2nd European Conference on Earthquake Engineering and Seismology, Istabul*.

RUV. (2022a). *https://www.ruv.is/frett/2022/07/31/skemmdir-a-vatnsleidslu-i-grindavik-ekkert-kalt-vatn*. accessed 25 November 2022.

RUV. (2022b). *https://www.ruv.is/frett/2022/07/31/tilkynnt-um-tjon-vegna-skjalftans-i-grindavik*. accessed 25 November 2022.

Sæmundsson, K., Sigurgeirsson, M. Á., Hjartarson, Á., Kaldal, I., Kristinsson, S. G., & Víkingsson, S. (2016). *Geological map of Southwest Iceland, 1: 100 000 (2nd edition)*. Reykjavík: Icelandic Energy Research.

Sæmundsson, K., Sigurgeirsson, M., & Friðleifsson, G. Ó. (2020). Geology and structure of the Reykjanes volcanic system, Iceland. *Journal of Volcanology and Geothermal Research*, *391*, 106501. https://doi.org/10.1016/j.jvolgeores.2018.11.022

SI. (2010). Icelandic National Annexes to Eurocodes. *Standards Council of Iceland / Stadlarad Íslands*.

Sigmundsson, F., Einarsson, P., Hjartardóttir, Á. R., Drouin, V., Jónsdóttir, K., Árnadóttir, T., Geirsson, H., Hreinsdóttir, S., Li, S., & Ófeigsson, B. G. (2020). Geodynamics of Iceland and the signatures of plate spreading. *Journal of Volcanology and Geothermal Research*, *391*, 106436. https://doi.org/10.1016/j.jvolgeores.2018.08.014

Sigmundsson, F., Parks, M., Hooper, A., Geirsson, H., Vogfjörd, K. S., Drouin, V., Ófeigsson, B. G., Hreinsdóttir, S., Hjaltadóttir, S., Jónsdóttir, K., Einarsson, P., Barsotti, S., Horálek, J., & Ágústsdóttir, T. (2022). Deformation and seismicity decline before the 2021 Fagradalsfjall eruption. *Nature*. https://doi.org/10.1038/s41586-022-05083-4

Stefánsson, R., Böðvarsson, R., Slunga, R., Einarsson, P., Jakobsdóttir, S., Bungum, H., Gregersen, S., Havskov, J., Hjelme, J., & Korhonen, H. (1993). Earthquake prediction research in the South Iceland Seismic Zone and the SIL Project N. *Bulletin of the Seismological Society of America*, *83*(3), 696–716.

Tusa, G., & Langer, H. (2016). Prediction of ground motion parameters for the volcanic area of Mount Etna. *Journal of Seismology*, *20*(1), 1–42. https://doi.org/10.1007/s10950-015-9508-x

Tusa, G., Langer, H., & Azzaro, R. (2020). Localizing ground-motion models in volcanic terranes: Shallow events at mt. etna, Italy, revisited. *Bulletin of the Seismological Society of America*, *110*(6), 2843–2861. https://doi.org/10.1785/0120190325

United States Geological Survey, U. (2022). *Earthquake Catalog*. accessed 20 November 2022 at URL https://earthquake.usgs.gov/earthquakes/search/.

Wiemer, S., & Wyss, M. (2000). Minimum Magnitude of Completeness in Earthquake Catalogs: Examples from Alaska, the Western United States, and Japan. In *Bulletin of the Seismological Society of America* (Vol. 90).